The Bacteriophage T7 Virion Undergoes Extensive Structural Remodeling During Infection

Bo Hu *et al.*

Science **339**, 576 (2013);
DOI: 10.1126/science.1231887

To illustrate the first mechanism, consider a scenario where a polarized group is travelling perpendicular to a gradient in light level. Individuals within the group, if located on the brighter side of the environment, will travel more quickly. This, in conjunction with interindividual attraction, induces rotation and turning toward the darker region. We find that, for a single instance in time, variation in speed among fish within a group corresponds to the variation in light level at their locations (Fig. 2A, dashed line). This speed differential across a group causes turning toward those who move more slowly (fig. S10). Second, as individuals slow down, the distance between them is reduced (see fig. S14), which increases the local density of animals in darker regions. Social influence results in acceleration tending to be in this direction (Fig. 2B).

To demonstrate the generic nature of these results, we performed simulations of grouping individuals (*17*, *18*) that moderate their speed according to their local light level. Simulated individuals move within the same light fields that were presented to the real fish, yet lack any explicit gradient detection capacity. As in the experiments, greater group-level responsiveness to the environment arises spontaneously as group size increases (Fig. 1B). Further, we show that, although increased group numbers reduce measurement error, the key determinant of performance is the spatial extent of the group in relation to the length scale of the environment; groups that span a larger area are more likely to capture the variation in cue required to elicit a speed differential across the group (*16*).

Motion toward darker regions (taxis), therefore, results from social interactions among individuals, each of whom exhibits a rudimentary, nondirectional response to their environment (kinesis). Thus, the collective dynamics create a group-level responsiveness to the environment that is absent at the individual level (*19*). The resulting increase in gradient-tracking ability for larger groups agrees with previous hypotheses (*20*, *21*) and could explain empirical studies showing that grouping facilitates the detection of chemical cues (*22*–*24*) and improves the accuracy of migrations that rely on such cues (*25*, *26*).

The simple algorithm revealed here may allow groups to respond to environmental gradients that occur over long length scales, for instance during the seasonal migration of fish tracking a single isotherm (*27*). If the mechanism we observed here is found to be widespread, as would be suggested by its robust nature and ease of implementation (in evolutionary terms), there are important ramifications for ecosystem conservation and management. Our results demonstrate that the ability to respond to environmental information may decline as populations are fragmented and average group sizes decrease.

References and Notes

1. A. W. Woolley, C. F. Chabris, A. Pentland, N. Hashmi, T. W. Malone, *Science* **330**, 686 (2010).
2. D. Grünbaum, *Evol. Ecol.* **12**, 503 (1998).
3. A. M. Simons, *Trends Ecol. Evol.* **19**, 453 (2004).
4. E. A. Codling, J. W. Pitchford, S. D. Simpson, *Ecology* **88**, 1864 (2007).
5. P. A. Larkin, A. Walton, *J. Fish. Res. Board Can.* **26**, 1372 (1969).
6. C. W. Clark, M. Mangel, *Theor. Popul. Biol.* **30**, 45 (1986).
7. I. D. Couzin *et al.*, *Science* **334**, 1578 (2011).
8. N. R. Franks, S. C. Pratt, E. B. Mallon, N. F. Britton, D. J. Sumpter, *Phil. Trans. R. Soc. B* **357**, 1567 (2002).
9. F. Galton, *Nature* **75**, 450 (1907).
10. S. Bauer *et al.*, in *Animal Migration: A Synthesis*, E. J. Milner-Gulland, J. M. Fryxell, A. R. E. Sinclair, Eds. (Oxford Univ. Press, New York, 2011), pp. 68–87.
11. T. J. Pitcher, J. K. Parrish, *Behaviour of Teleost Fishes* (Springer, New York, 1993), vol. 2, pp. 369–439.
12. R. Poli, J. Kennedy, T. Blackwell, *Swarm Intell.* **1**, 33 (2007).
13. P. Ogren, E. Fiorelli, N. E. Leonard, *IEEE Trans. Automat. Contr.* **49**, 1292 (2004).
14. S. G. Reebs, *Anim. Behav.* **59**, 403 (2000).
15. D. J. Hall *et al.*, *J. Fish. Board Can.* **36**, 1029 (1979).
16. Materials and methods are available as supplementary materials on *Science* Online.
17. I. D. Couzin, J. Krause, N. R. Franks, S. A. Levin, *Nature* **433**, 513 (2005).
18. M. Camperi, A. Cavagna, I. Giardina, G. Parisi, E. Silvestri, *Interface Focus* **2**, 715 (2012).
19. C. J. Torney, Z. Neufeld, I. D. Couzin, *Proc. Natl. Acad. Sci. U.S.A.* **106**, 22055 (2009).
20. A. Huth, C. Wissel, *Ecol. Modell.* **75-76**, 135 (1994).
21. U. Kils, thesis, University of Kiel, Germany (1987).
22. R. E. McNicol, E. Scherer, J. H. Gee, *Environ. Biol. Fishes* **47**, 311 (1996).
23. L. W. Hall Jr., D. T. Burton, S. L. Margrey, W. C. Graves, *J. Toxicol. Environ. Health* **10**, 1017 (1982).
24. C. W. Steele, A. D. Scarfe, D. W. Owens, *J. Fish Biol.* **38**, 553 (1991).
25. T. P. Quinn, K. Fresh, *Can. J. Fish. Aquat. Sci.* **41**, 1078 (1984).
26. J. J. Hard, W. R. Heard, *Can. J. Fish. Aquat. Sci.* **56**, 578 (1999).
27. K. Schaefer, D. Fuller, B. Block, *Mar. Biol.* **152**, 503 (2007).

Acknowledgments: We thank J. Herbert-Read for experimental assistance, N. O. Handegard for providing code and advice for track linking, and A. Haenssen for technical support. Suggestions from members of the Couzin laboratory and two anonymous reviewers greatly improved this manuscript. Funded by NSF awards PHY-0848755, EAGER-1251585, and CNH-1211972; U.S. Office of Naval Research award N00014-09-1-1074; U.S. Army Research Office grant W911NG-11-1-0385; Leverhulme Early Career Fellowship; Natural Sciences and Engineering Research Council of Canada Postgraduate Scholarship Fellowship; and the Yukon Foundation. All experiments were conducted in accordance with federal and state regulations and were approved by the Princeton University Institutional Animal Care and Use Committee. Code freely available at http://icouzin.princeton.edu.

Supplementary Materials

www.sciencemag.org/cgi/content/full/339/6119/574/DC1
Materials and Methods
Supplementary Text
Figs. S1 to S17
Tables S1 and S2
References (*28*–*30*)

11 June 2012; accepted 12 December 2012
10.1126/science.1225883

The Bacteriophage T7 Virion Undergoes Extensive Structural Remodeling During Infection

Bo Hu,[1] William Margolin,[2] Ian J. Molineux,[3]* Jun Liu[1]*

Adsorption and genome ejection are fundamental to the bacteriophage life cycle, yet their molecular mechanisms are not well understood. We used cryo–electron tomography to capture T7 virions at successive stages of infection of *Escherichia coli* minicells at ~4-nm resolution. The six phage tail fibers were folded against the capsid, extending and orienting symmetrically only after productive adsorption to the host cell surface. Receptor binding by the tail triggered conformational changes resulting in the insertion of an extended tail, which functions as the DNA ejection conduit into the cell cytoplasm. After ejection, the extended phage tail collapsed or disassembled, which allowed resealing of the infected cell membrane. These structural studies provide a detailed series of intermediates during phage infection.

After encountering a cell, a bacteriophage delivers its genetic material into the host cytoplasm via an orchestrated series of conformational changes (*1*). T7 is a member of the *Podoviridae*, having short, noncontractile tails that are too short to span a bacterial cell envelope (*2*). The icosahedral 2-nm-thick T7 capsid is 60 to 61 nm in diameter, and inside, coaxial to the dodecameric head-tail connector, is a 26- by 21-nm internal core, which is thought to consist of three proteins: gp14, gp15, and gp16 (*2*, *3*). The core is essential for both virion morphogenesis and ejection of the 40-kb genome. Near the head-proximal end of the 23-nm tail are six fibers, trimers of gp17. Each fiber has an N-terminal domain that attaches the fiber to the tail, followed by proximal and distal half-fibers. The latter interact with the cell surface (*4*, *5*). After adsorption, the core proteins are ejected through the portal-tail

[1]Department of Pathology and Laboratory Medicine, University of Texas Medical School at Houston, Houston, TX 77030, USA. [2]Department of Microbiology and Molecular Genetics, University of Texas Medical School at Houston, Houston, TX 77030, USA. [3]Molecular Genetics and Microbiology, Institute for Cell and Molecular Biology, University of Texas at Austin, Austin, TX 78712, USA.

*To whom correspondence should be addressed. E-mail: molineux@austin.utexas.edu (I.J.M.); jun.liu.1@uth.tmc.edu (J.L.)

complex into the infected cell, and it has been hypothesized that they extend the tail, creating a trans-envelope channel used for DNA transport (*6*–*8*). Here, we used cryo–electron tomography (cryo-ET) to provide three-dimensional (3D) structures of infected cell complexes in near-native, frozen-hydrated states at ~4-nm resolution (fig. S1).

We infected small (≤0.3 μm in diameter) *Escherichia coli* minicells (*9*) to achieve maximum resolution. The T7-infected minicells produced infective centers at normal efficiencies, and the parent skinny cells were good hosts for the phage, which suggested that our structures reflected the normal infection pathway (*10*). The 3D reconstructions revealed adsorbed virions at three stages of infection (Fig. 1 and movie S1) and supported the hypothesis (*6*–*8*) that T7 internal core proteins form a trans-envelope channel (Fig. 1, B and E). Dual-axis tomography confirmed the presence of various conformations (movie S2). In order to obtain better structural details, we used subvolume averaging to determine the 3D structures during infection (*10*).

Asymmetric reconstructions of a fiberless gene *17* mutant (Fig. 2, A and D) and wild-type (Fig. 2, B and E) virions were derived from 1945 and 6116 subvolumes, respectively. The overall structure of wild-type T7 (Fig. 2B) is similar to that reported (*3*), but our tomographic reconstruction resolved the tail fibers (Fig. 2, B, C, E, and F). Placing a known structure of part of the distal half-fiber (*5*) into the cryo-ET density revealed a good fit (Fig. 2F). Each fiber was folded back onto the capsid with the proximal half-fiber rising across the face of a capsomer. The ~90° kink between proximal and distal half-fibers was visible in 3D surface renderings (Fig. 2, E and F). Fibers retained a conformation similar to that of isolated tail complexes (fig. S2) (*4*).

The T7 tail exhibited 6-fold symmetry, but the distal half-fibers were bound to the capsid, which is 5-fold symmetrical at the connector. To better understand the symmetry mismatch and the fiber-capsid interactions, we classified each fiber independently by correspondence analysis (figs. S3 and S4). Class I fibers exhibited only a short fragment corresponding to the N-terminal domain that is bound to the tail (*4*), which indicated that neither half-fiber was bound to the capsid. Proximal and distal half-fibers were visible in class II and were subdivided into subclasses by their different orientations on the capsid (Fig. 2, H and I). Projecting all distal half-fiber conformations onto the same surface showed that there is no specific binding site (fig. S4).

Phage tail fibers are normally depicted extending away from the capsid, poised for adsorption. However, we found that ~50% of mature T7 virions had five fibers bound to the capsid and ~30% had four; very few had no bound fibers (Fig. 2J). Most published electron microscopy (EM) images of T7 do not resolve fibers; they were visible in a tomogram of negatively stained T7 particles only as short projections from the capsid (fig. S2). More than 95% of the wild-type T7 prepared for this study made infective centers in exponentially growing cells within 2 to 3 min, which suggested that extended fibers were not required for rapid adsorption (*10*). Proximal half-fibers of the T7-related phage P-SSP7 also appear bound in mature virions but are extended in spontaneously emptied free particles (*11*). Furthermore, cryo-EM reconstructions of T4 virions show fibers wrapped around the tail sheath, not pointing away from the capsid (*12*). Maintaining tail fibers on the body of free virions may thus be typical of many phages.

Adsorbed T7 virions were generally oriented perpendicular to the cell surface with the tail slightly indenting the outer membrane (Fig. 3, A and B; fig. S5; and movie S3), similar to adsorbed phage P-SSP7 (*11*). Proximal half-fibers extended horizontally, whereas distal half-fibers were vertical; bound fibers exhibited the same 6-fold symmetry as the tail, covering ~3000 nm^2 of the cell surface. During adsorption, fibers underwent a large rotation, which was probably due to the N-terminal domain pivoting on its connection to the tail (fig. S6). Two-thirds (3352) of adsorbed phages analyzed were captured at this intermediate stage, with the internal core remaining intact within the capsid, which suggests that recognition of the cell surface by all six fibers is insufficient to trigger later steps of infection.

About one-third (1886) of adsorbed particles displayed a tubelike extension of the tail that penetrated both cell membranes (Fig. 3, C and D; figs. S5 and S7; and movie S3). A functional extension of the T7 tail is essential for genome delivery into the host (*2*). The energy required for this dramatic change in structure must be stored in the virion, because cellular energy sources will not yet be accessible. The interaction between the tail and the outer membrane also changed, which presumably reflects the conformational changes that signal ejection of the internal core, which was no longer visible (Fig. 3, A and C). However, the head still appeared full, which suggested that the encapsidated DNA had expanded to occupy the volume originally occupied by the core.

The extended tail is probably composed of ejected core proteins, which have been found in the infected cell envelope (*7*, *8*). Gp14 localizes to the infected cell outer membrane, whereas gp15 and gp16 span the periplasm and cytoplasmic membrane. Various mutant gp16-containing virions change the kinetics of genome ejection or prevent DNA from entering the cytoplasm; the latter defect can be suppressed by virions also harboring a mutant gp15 (*8*, *13*–*16*). After infection by *16E37F* mutant virions, which are defective in cell wall hydrolysis and which exhibit delayed DNA entry into the cytoplasm (*14*, *17*), the extended tail took ~20 times as long to form (fig. S8). The estimated volume of the internal core (*3*) is sufficient to form the entire extension. The overall tail extension was ~45 nm, and the tube had an outer diameter of

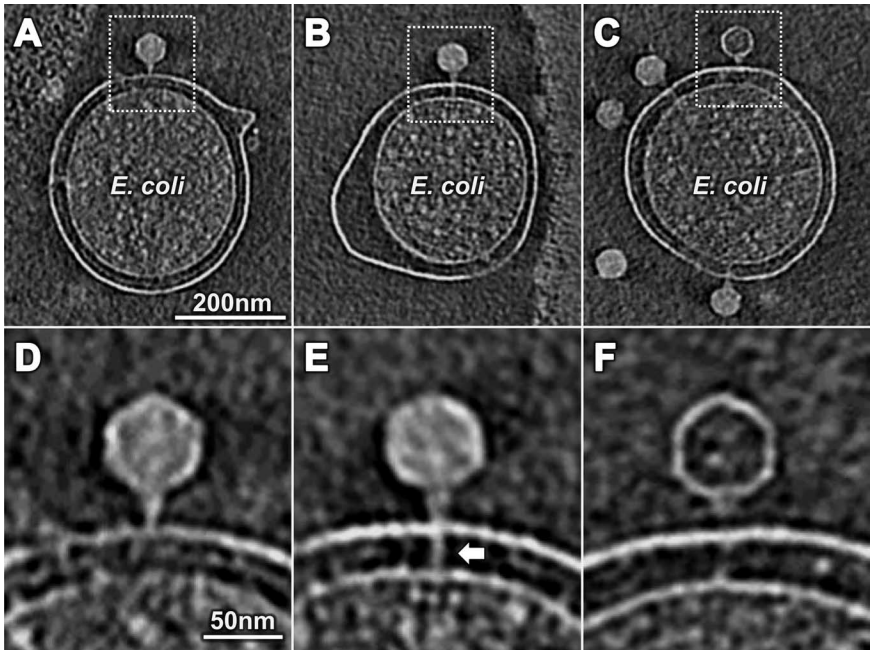

Fig. 1. Three stages of T7 infection. (**A** and **D**) T7 adsorbed to the outer membrane. The density spanning the cell envelope at 270° in (A) was derived from fiducial gold markers (shown explicitly in movie S1 as a series of slices across the cell in (A). (**B** and **E**) An extended tail (arrow) spanned the cell envelope. (**C** and **F**) After DNA ejection, the extended tail was not apparent.

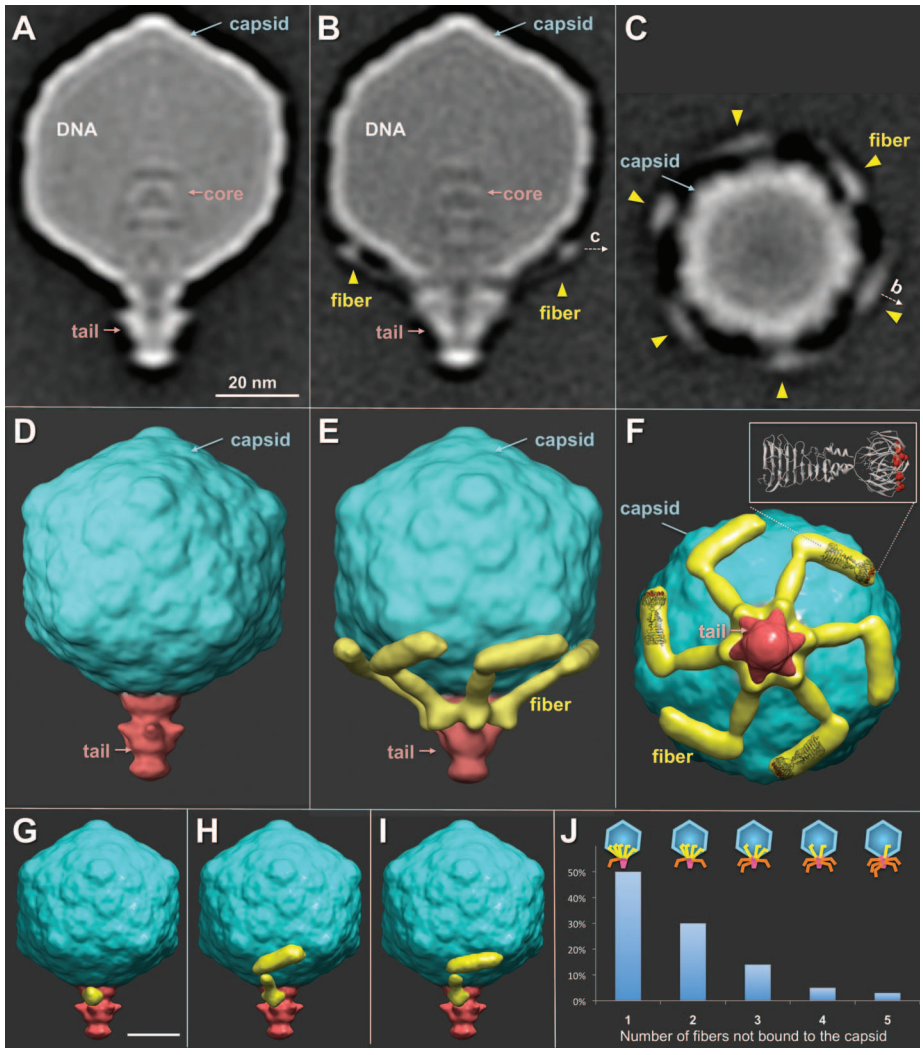

Fig. 2. Asymmetric reconstructions of virions. (**A**) A central slice of a fiberless virion revealed the tail, capsid, and internal core. Fibers were visible in a central slice (**B**) and a cross section of wild-type virions (**C**). Surface rendering of fiberless (**D**) and wild-type virions in side (**E**) and bottom (**F**) views. A crystal structure of the receptor-binding domain of T7 fibers (*5*) was placed into three fiber densities. Residues A518, D520, and V544, known to affect phage host range (*5*), are highlighted in red (F). Classification revealed different conformations of fibers not bound (**G**) or bound to the capsid (**H** and **I**). (**J**) Distribution of the number of bound fibers on free virions; few had either six or zero fibers bound.

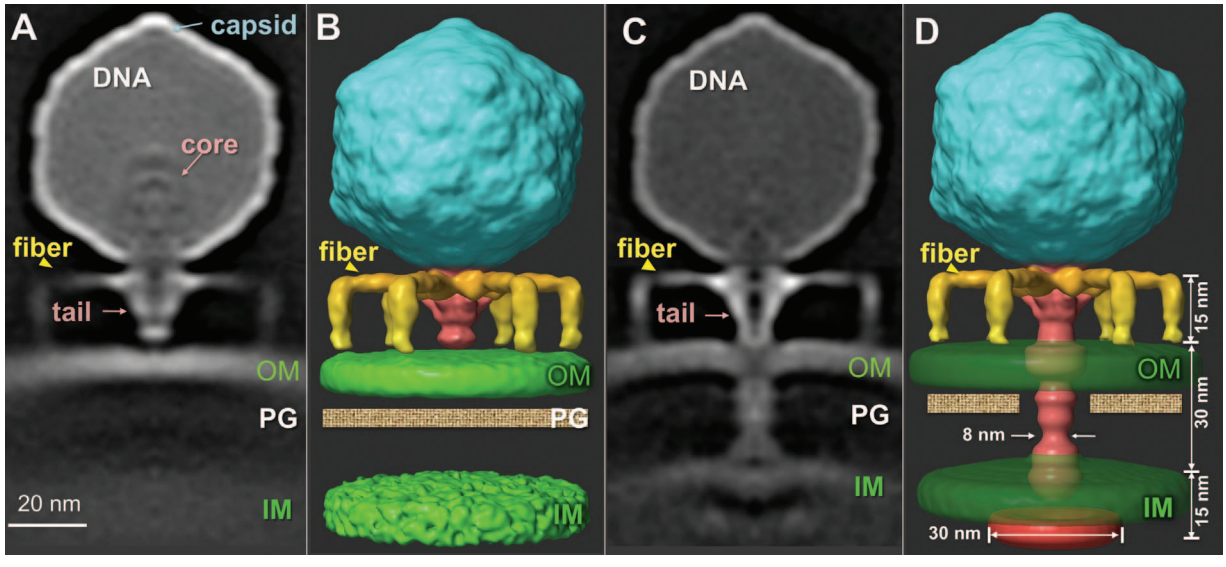

Fig. 3. Adsorption structures. (**A**) Central slice and (**B**) 3D surface view of a subvolume average derived from 3352 virions. All six fibers were bound to the cell, and the tail made a small indentation in the outer membrane (OM); the internal core and DNA were still in the capsid. (**C**) Central slice and (**D**) 3D surface view of a subvolume average derived from 1886 virions. The internal core had been ejected from the virion, forming an extended tail that penetrated the cell cytoplasm. PG, peptidoglycan cell wall; IM, inner membrane.

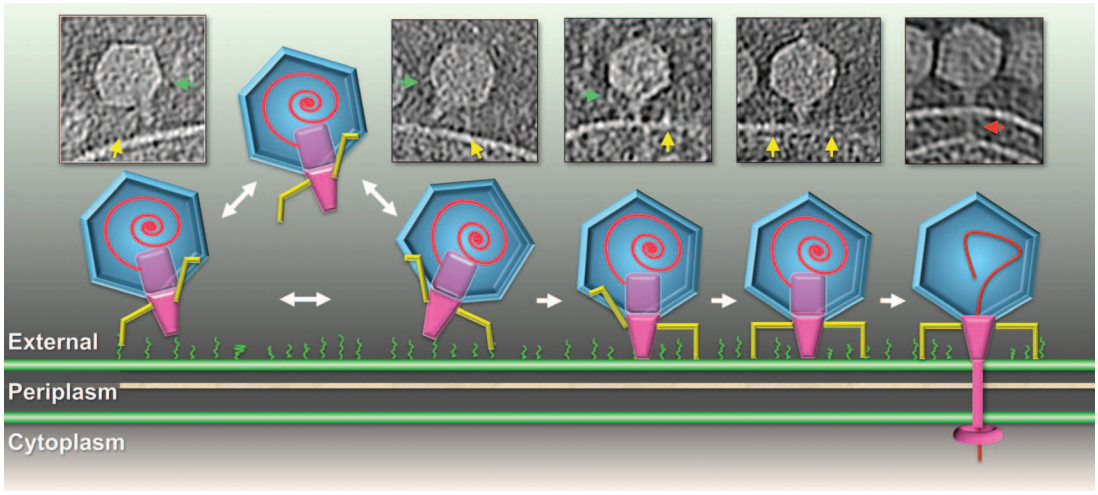

Fig. 4. Schematic model of T7 infection. The insert tomograms show the different orientations of tail fibers. Fibers bound to the cell are highlighted with yellow arrows, unbound fibers with green arrows. After "walking" across the cell surface to find the receptor for the tail, all fibers rotate downward to contact the outer membrane. Commitment to infection occurs after internal core proteins are ejected from the virion and the extended tail (red arrow) forms.

≥8 nm, sufficient to accommodate double-stranded DNA in its lumen. As the tube approached the cytoplasmic membrane, density broadened (Fig. 3, C and D), probably because the extended tail was flexible (movie S4). Density associated with the tube was less distinct inside the cytoplasm, but ~12 nm below the center of the membrane a ~30 by 6 nm toroid with a ~4-nm central cavity was clearly present (fig. S9 and movie S4). The toroid may be part of the molecular motor that has been hypothesized to pull the leading genome end into the cell (*6*, *8*, *16*).

About 3% (162) of adsorbed phages had completely ejected their genome. Virion structure at this stage of infection was thus determined only at relatively low resolution (fig. S10 and movie S3). The cytoplasmic toroid was not visible, and the tube traversing the periplasm had collapsed or disassembled, which presumably prevented dissipation of the membrane potential, which would inhibit phage development. We tested whether an energized membrane was required for channel formation by treating minicells with carbonyl cyanide *m*-chlorophenyl hydrazone (CCCP) before infection. Of the 244 virions observed, 14% did not adsorb, 55% adsorbed without tail extension, 31% formed a trans-envelope structure, but none ejected their genome (fig. S11). An energized membrane was thus not necessary for adsorption or ejection of internal proteins, but, as expected (*16*, *18*), it is essential for genome translocation.

The combination of technical advances in cryo-ET and a reduction in *E. coli* cell size has allowed us to describe detailed features of the mature T7 virion and structural changes during infection. Tail fibers, usually depicted extending away from the virion, were mostly bound to the capsid. Our data suggest a dynamic equilibrium between bound and unbound states. Maintaining fibers in a folded-back configuration would allow a higher rate of virion diffusion, whereas transient extension could still permit the phage to explore a large volume in search of a cell. Binding of fibers to bacterial receptors is weak, but transient binding could reduce the dimensional space for finding a suitable site for infection from three to two (*19*). Weak binding could potentially achieve the necessary specificity of adsorption by cooperative binding among fibers or by a second component, i.e., the tail, binding with high specificity (*2*, *7*, *20*). We propose that the transition to a stably adsorbed state occurs following a random walk after an initial interaction between a fiber and the cell; e.g., bound fiber no. 1 is directly replaced by binding of fiber no. 2 without virion release (Fig. 4 and movie S5). Alternatively, in a quasi-2D diffusion process, fiber no. 1 may dissociate, followed rapidly by fiber no. 2 detaching from the capsid and binding to the cell. Note that the common lab strain of phage λ, which lacks side tail fibers, has been suggested to move across the cell surface in a quasi-1D process (*21*). At a preferred site of infection, the tail interacts specifically with its receptor, which prevents further lateral movement and allows all fibers to bind. The fibers of phage T7 may thus function primarily to facilitate interaction of the tail with its specific receptor. After stable adsorption, infection is triggered by ejection of the internal core proteins into the cell envelope and the formation of an extended tail, which may protect the entering genome from periplasmic nucleases.

References and Notes

1. J. E. Johnson, W. Chiu, *Curr. Opin. Struct. Biol.* **17**, 237 (2007).
2. S. R. Casjens, I. J. Molineux, *Adv. Exp. Med. Biol.* **726**, 143 (2012).
3. X. Agirrezabala *et al.*, *EMBO J.* **24**, 3820 (2005).
4. A. C. Steven *et al.*, *J. Mol. Biol.* **200**, 351 (1988).
5. C. Garcia-Doval, M. J. van Raaij, *Proc. Natl. Acad. Sci. U.S.A.* **109**, 9390 (2012).
6. I. J. Molineux, *Mol. Microbiol.* **40**, 1 (2001).
7. P. Kemp, L. R. Garcia, I. J. Molineux, *Virology* **340**, 307 (2005).
8. C. Y. Chang, P. Kemp, I. J. Molineux, *Virology* **398**, 176 (2010).
9. J. Liu *et al.*, *Proc. Natl. Acad. Sci. U.S.A.* **109**, E1481 (2012).
10. See supplementary materials on *Science* Online.
11. X. Liu *et al.*, *Nat. Struct. Mol. Biol.* **17**, 830 (2010).
12. P. G. Leiman *et al.*, *Virol. J.* **7**, 355 (2010).
13. L. R. García, I. J. Molineux, *J. Bacteriol.* **178**, 6921 (1996).
14. M. Moak, I. J. Molineux, *Mol. Microbiol.* **37**, 345 (2000).
15. J. S. Struthers-Schlinke, W. P. Robins, P. Kemp, I. J. Molineux, *J. Mol. Biol.* **301**, 35 (2000).
16. P. Kemp, M. Gupta, I. J. Molineux, *Mol. Microbiol.* **53**, 1251 (2004).
17. M. Moak, I. J. Molineux, *Mol. Microbiol.* **51**, 1169 (2004).
18. A. Z. Zimkus, S. K. Zavriev, L. L. Grinius, *Mol. Biol. (Mosk)* **20**, 185 (1986).
19. G. Adam, M. Delbrück, in *Structural Chemistry and Molecular Biology*, R. Rich, N. Davidson, Eds. (Freeman, San Francisco, 1968), pp. 198–215.
20. U. Qimron, B. Marintcheva, S. Tabor, C. C. Richardson, *Proc. Natl. Acad. Sci. U.S.A.* **103**, 19039 (2006).
21. E. Rothenberg *et al.*, *Biophys. J.* **100**, 2875 (2011).

Acknowledgments: We thank P. Leiman, S. Norris, and Y. W. Yin for comments. B.H. and J.L. were supported in part by grants R01AI087946 from the National Institute on Allergy and Infection, NIH, and AU-1714 from the Welch Foundation. W.M. was supported by NIH grant R01GM61074 and a grant from the Human Frontier Science Program. EM maps have been deposited in the EM Data Bank (www.ebi.ac.uk/pdbe/emdb/) with accession nos. EMD-5534, 5535, 5536, and 5537. J.L. and I.J.M. designed research; B.H. and W.M. constructed the *E. coli* mutants; B.H. and J.L. collected and analyzed data; and B.H., W.M., J.L., and I.J.M. wrote the paper.

Supplementary Materials

www.sciencemag.org/cgi/content/full/science.1231887/DC1
Materials and Methods
Figs. S1 to S11
Table S1
References (*22*–*30*)
Movies S1 to S5

23 October 2012; accepted 13 December 2012
Published online 10 January 2013;
10.1126/science.1231887